Electronic Supplementary Material (ESI) for Dalton Transactions.

Supporting Information

Unsymmetrical Diarylamido-Based Rare-Earth Alkyl Complexes: Synthesis and Catalytic Performance in Isoprene Polymerization

Wenhui Ren[a], Hui Liu,[a] Fen You,[a] Pengjuan Mao,[b] Yat-Ming So,[c] Xiaohui Kang*[b] and Xiaochao Shi*[a]

[a]*Department of Polymer Materials, College of Materials Science and Engineering, Shanghai University, Materials Building, Nanchen Street 333, Shanghai 200444, China; E-mail: xcshi@shu.edu.cn*
[b]*College of Pharmacy, Institute of Integrative Medicine, Dalian Medical University, Dalian 116044, China.; E-mail: kangxh@dmu.edu.cn*
[c]*Department of Chemistry, The Hong Kong University of Science and Technology, Clear Water Bay, Kowloon, Hong Kong, China*

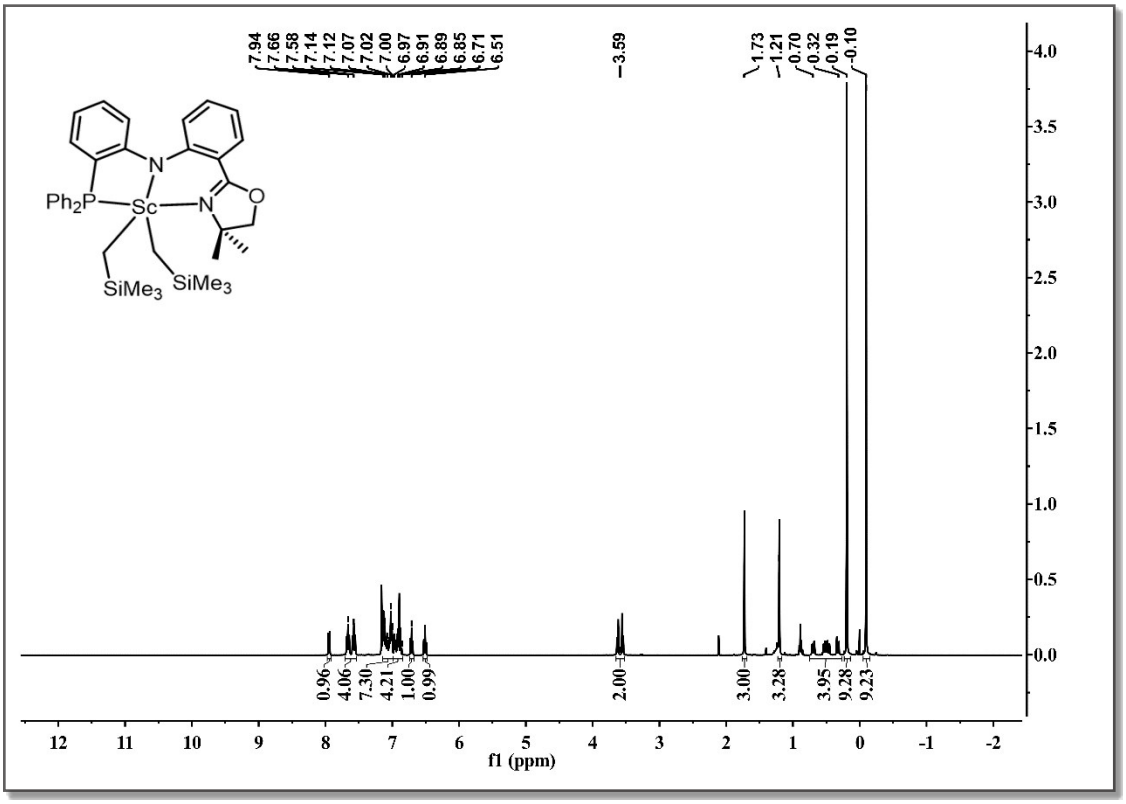

Figure S1 ^{1}H NMR spectrum of **P-Sc** (400 MHz, C_6D_6, 25 ^{o}C)

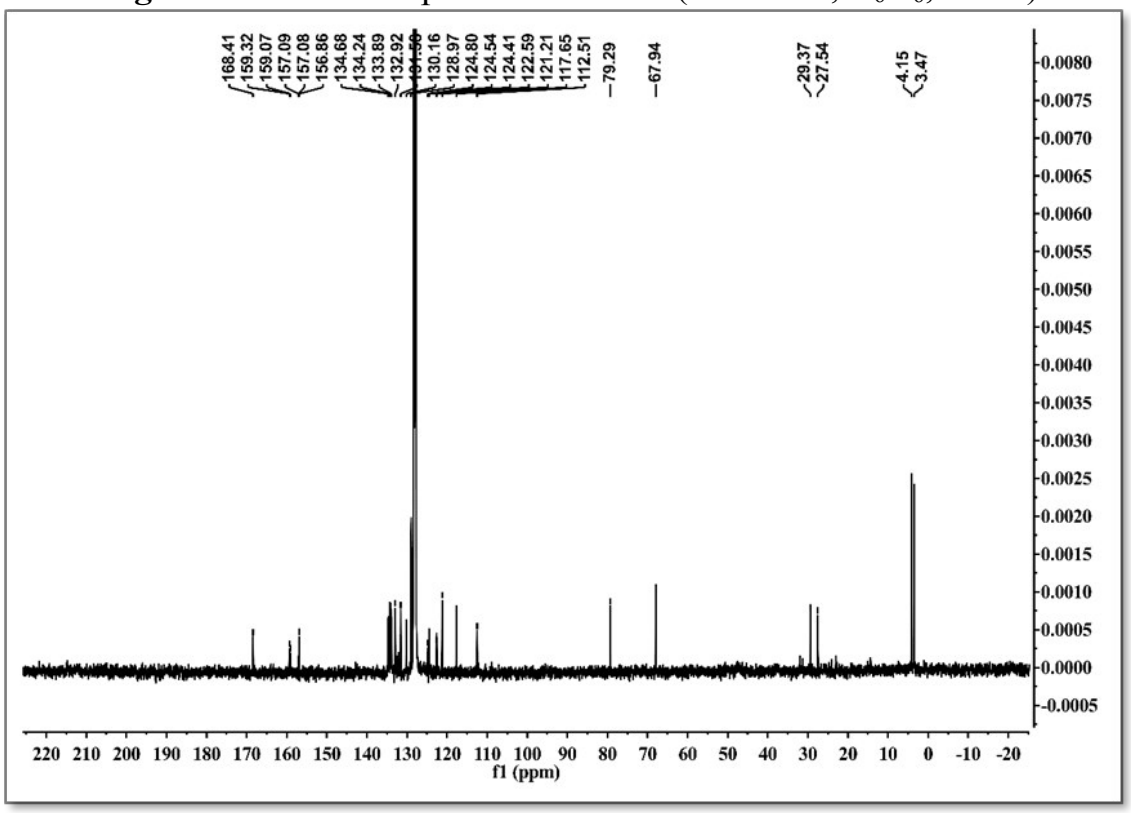

Figure S2 ^{13}C NMR spectrum of **P-Sc** (101 MHz, C_6D_6, 25 ^{o}C)

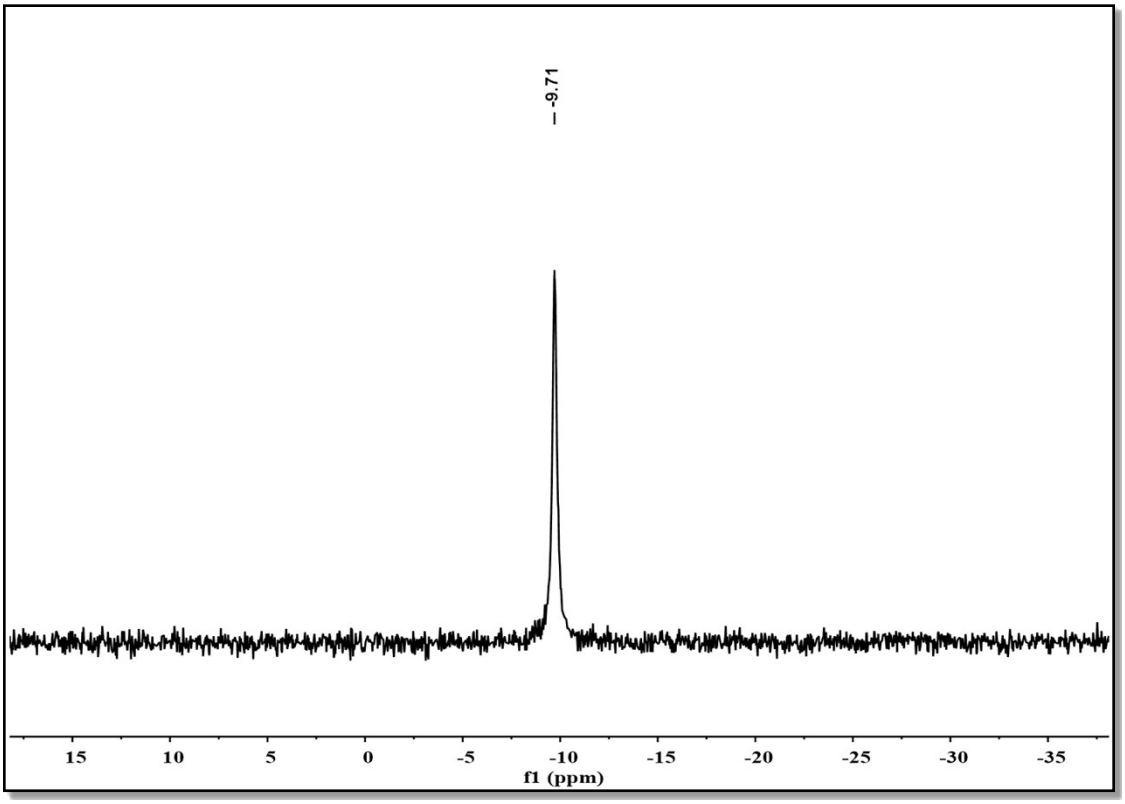

Figure S3 ^{31}P $\{^{1}H\}$ NMR spectrum of **P-Sc** (162 MHz, C_6D_6, 25 ^{o}C)

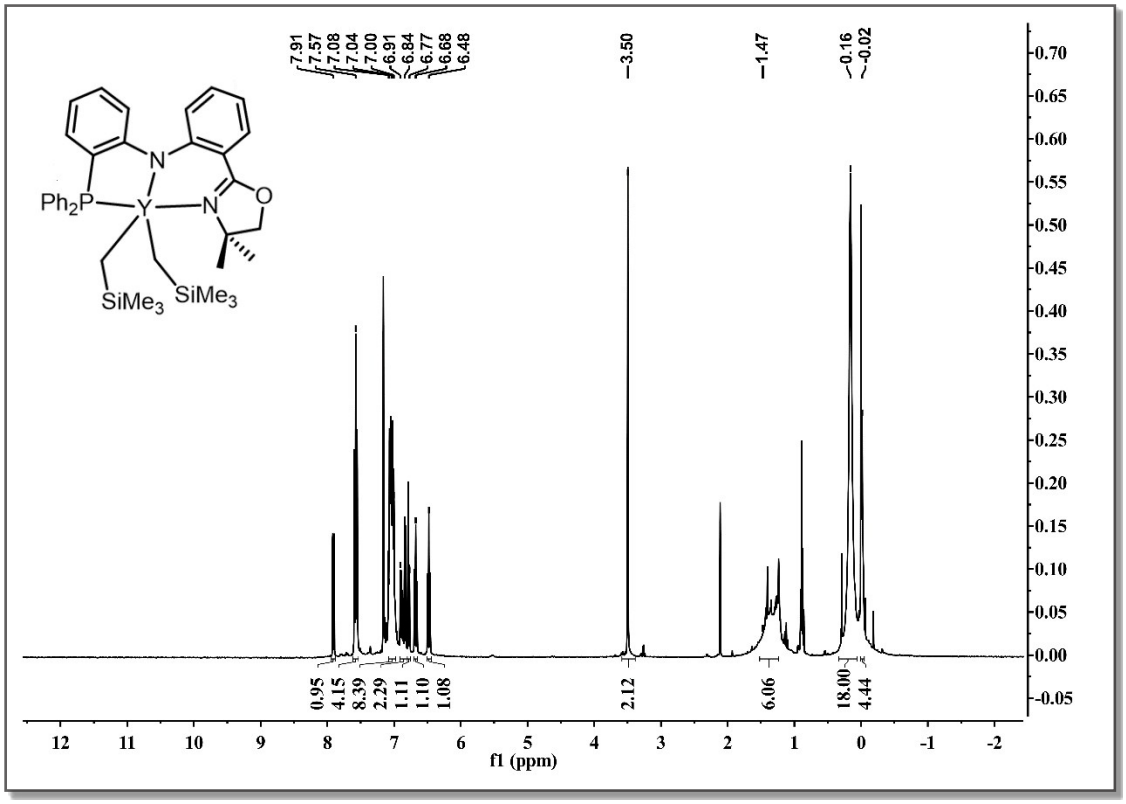

Figure S4 ^{1}H NMR spectrum of **P-Y** (400 MHz, C_6D_6, 25 ^{o}C)

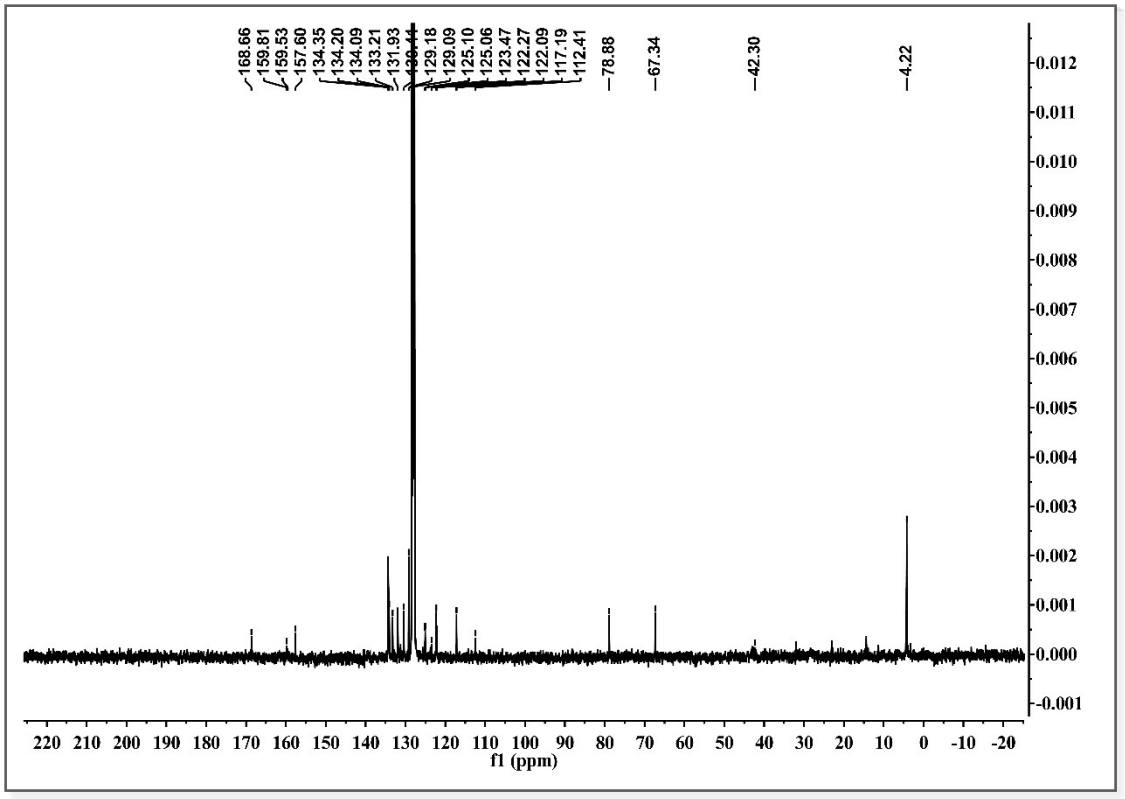

Figure S5 ^{13}C NMR spectrum of **P-Y** (101 MHz, C_6D_6, 25 ^{o}C)

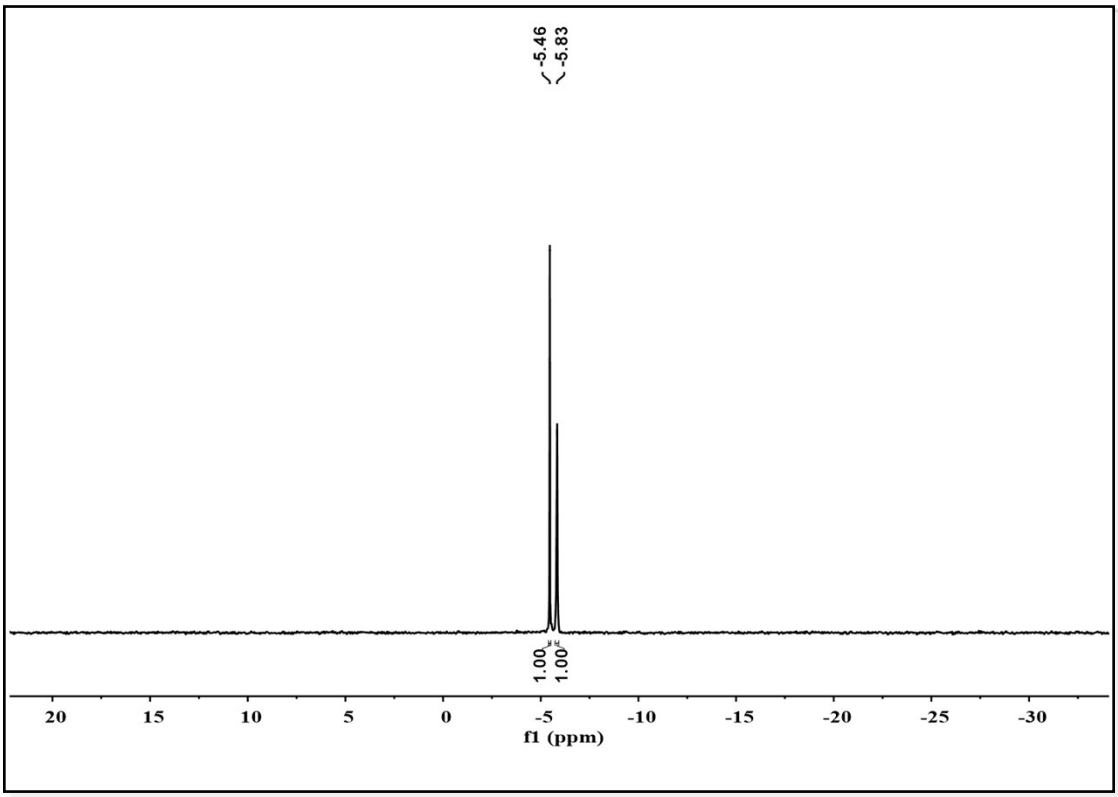

Figure S6 ^{31}P $\{^{1}H\}$ NMR spectrum of **P-Y** (162 MHz, C_6D_6, 25 ℃)

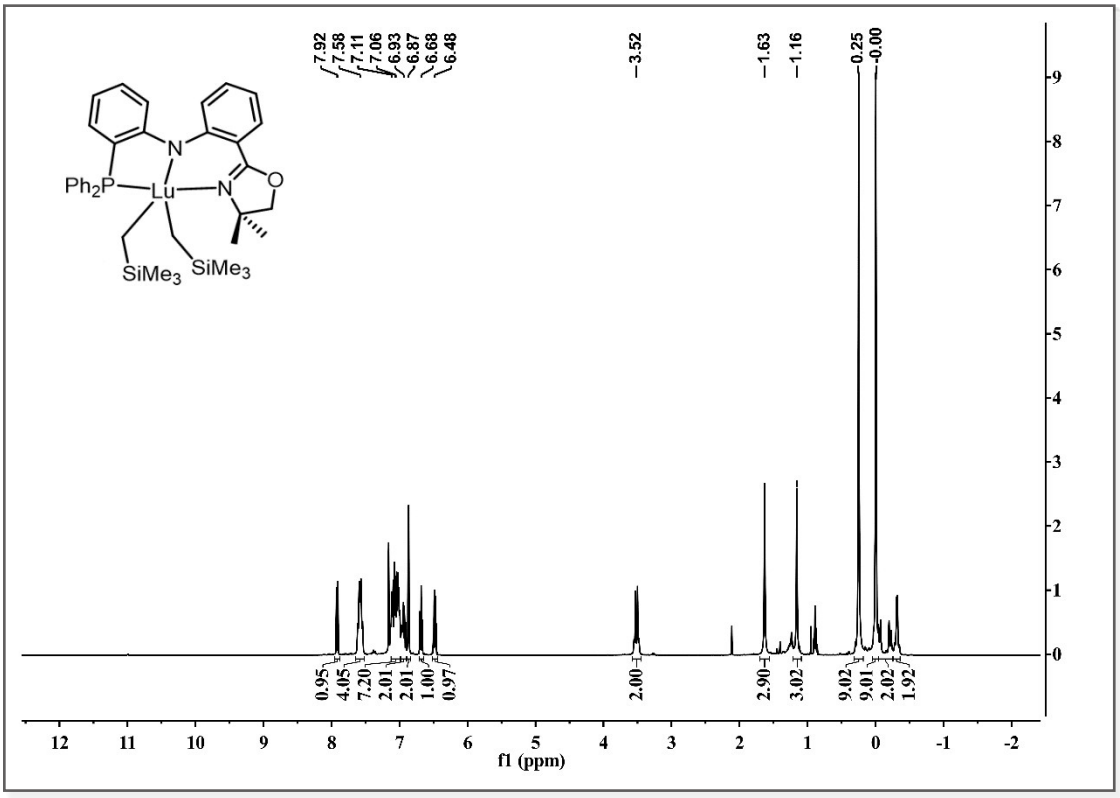

Figure S7 ^{1}H NMR spectrum of **P-Lu** (400 MHz, C_6D_6, 25 °C)

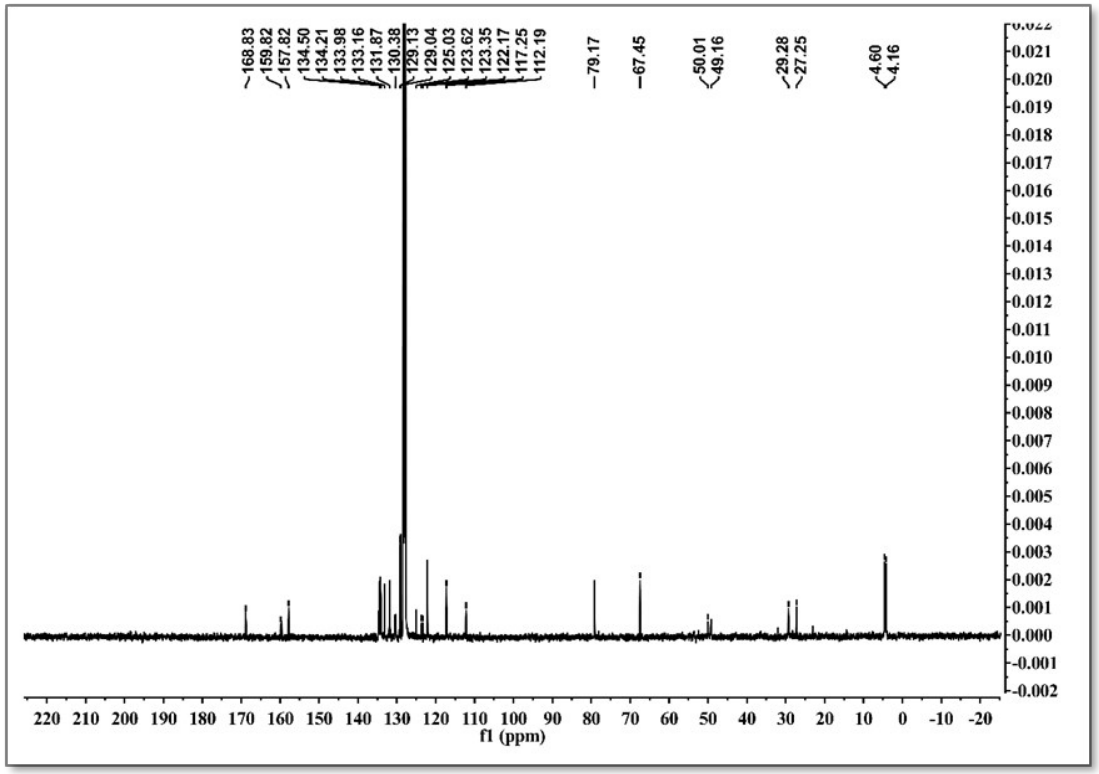

Figure S8 ^{13}C NMR spectrum of **P-Lu** (101 MHz, C_6D_6, 25 °C)

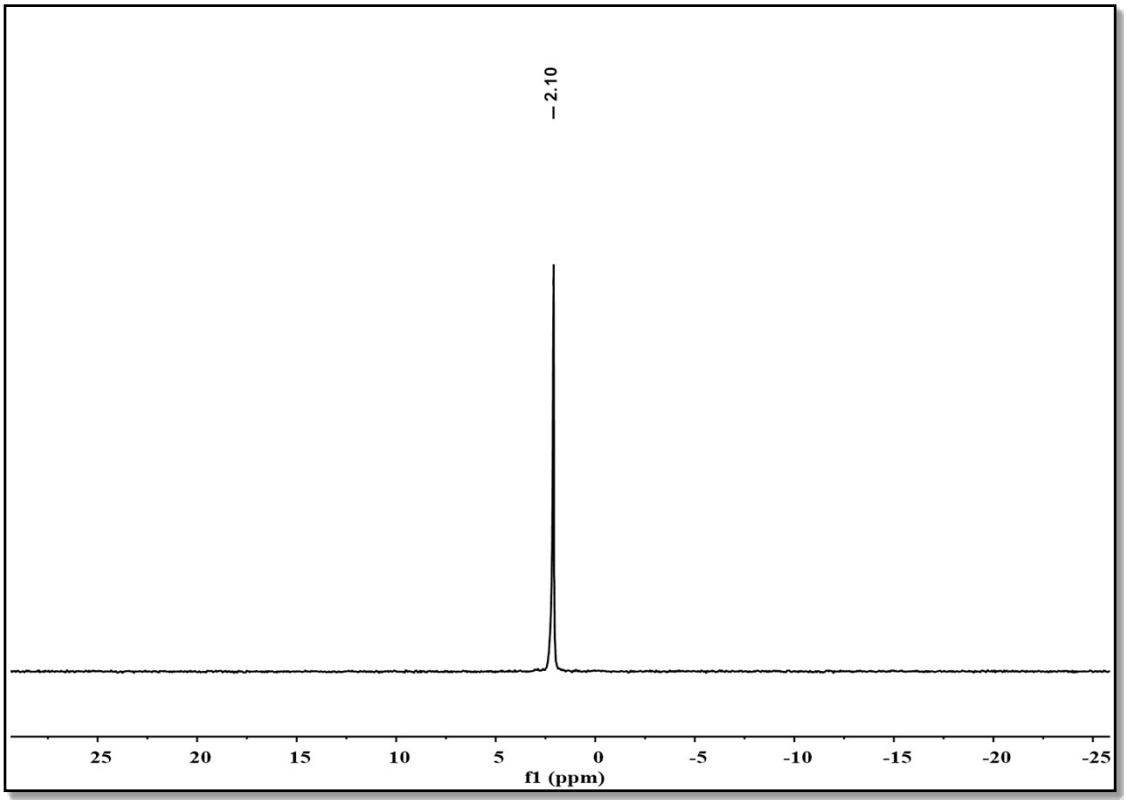

Figure S9 ^{31}P $\{^{1}H\}$ NMR spectrum of **P-Lu** (162 MHz, C_6D_6, 25 ℃)

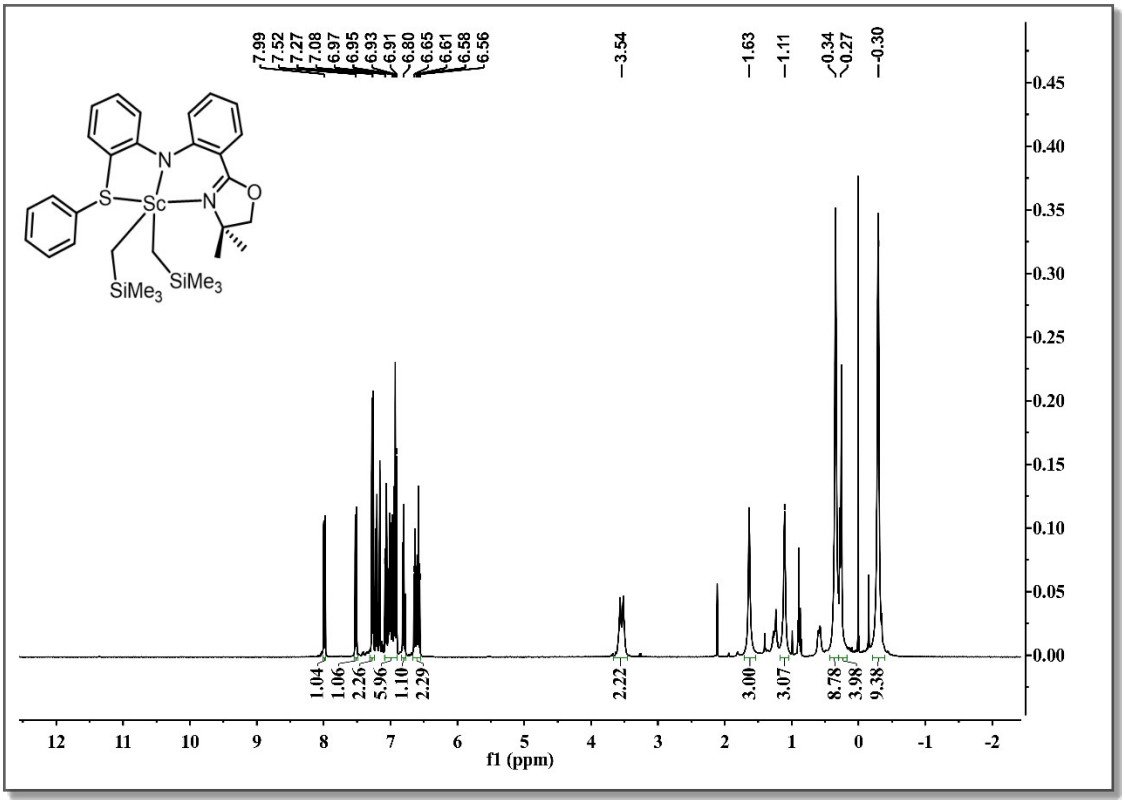

Figure S10 ^{1}H NMR spectrum of **S-Sc** (400 MHz, C_6D_6, 25 °C)

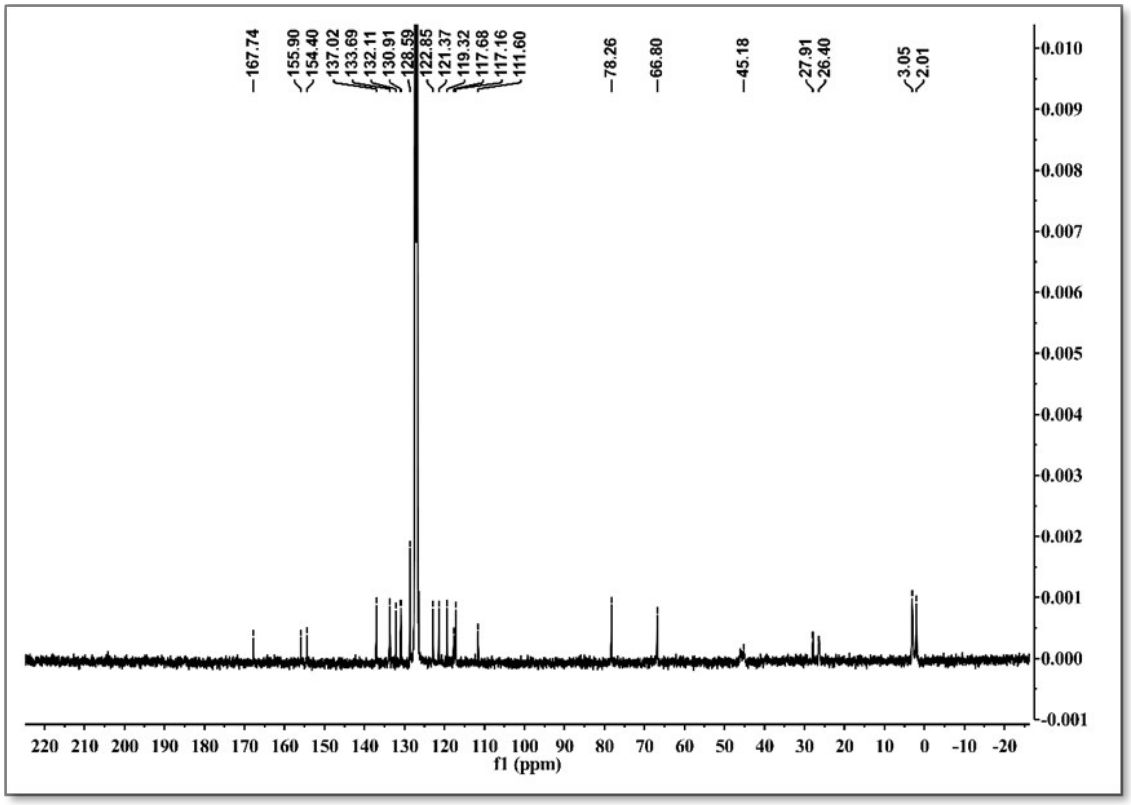

Figure S11 ^{13}C NMR spectrum of **S-Sc** (101 MHz, C_6D_6, 25 °C)

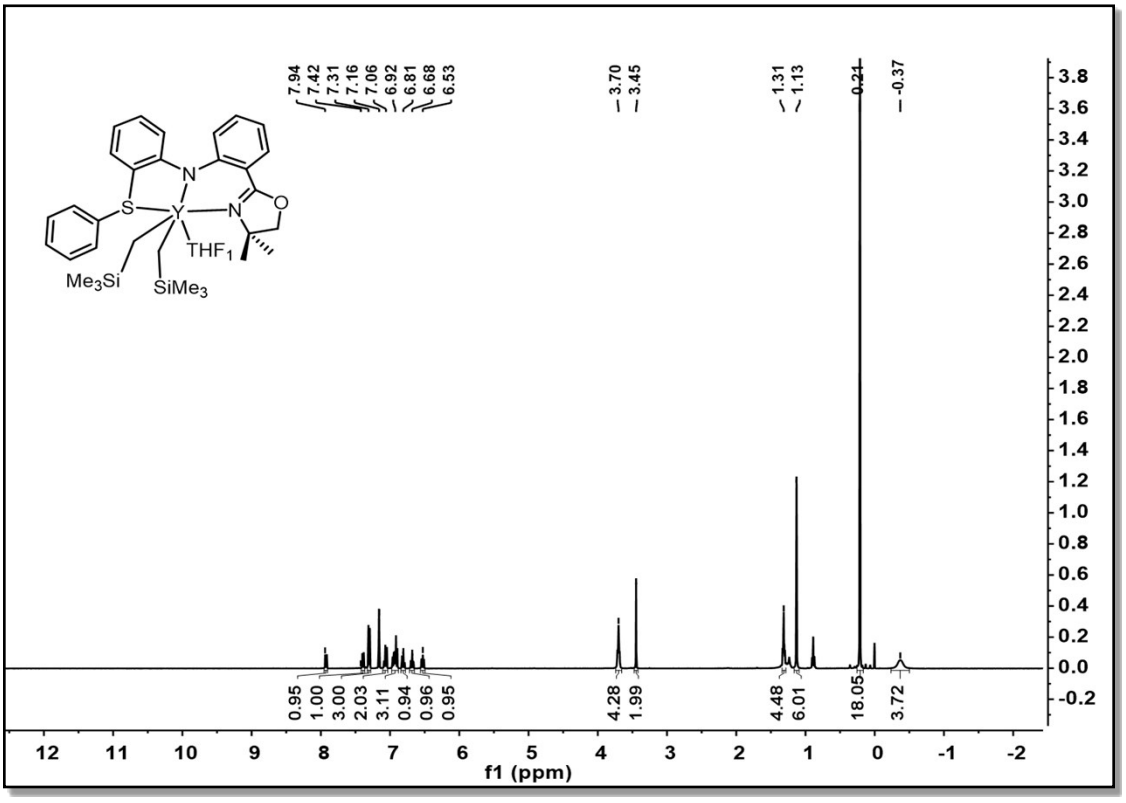

Figure S12 ^{1}H NMR spectrum of **S-Y** (400 MHz, C_6D_6, 25 °C)

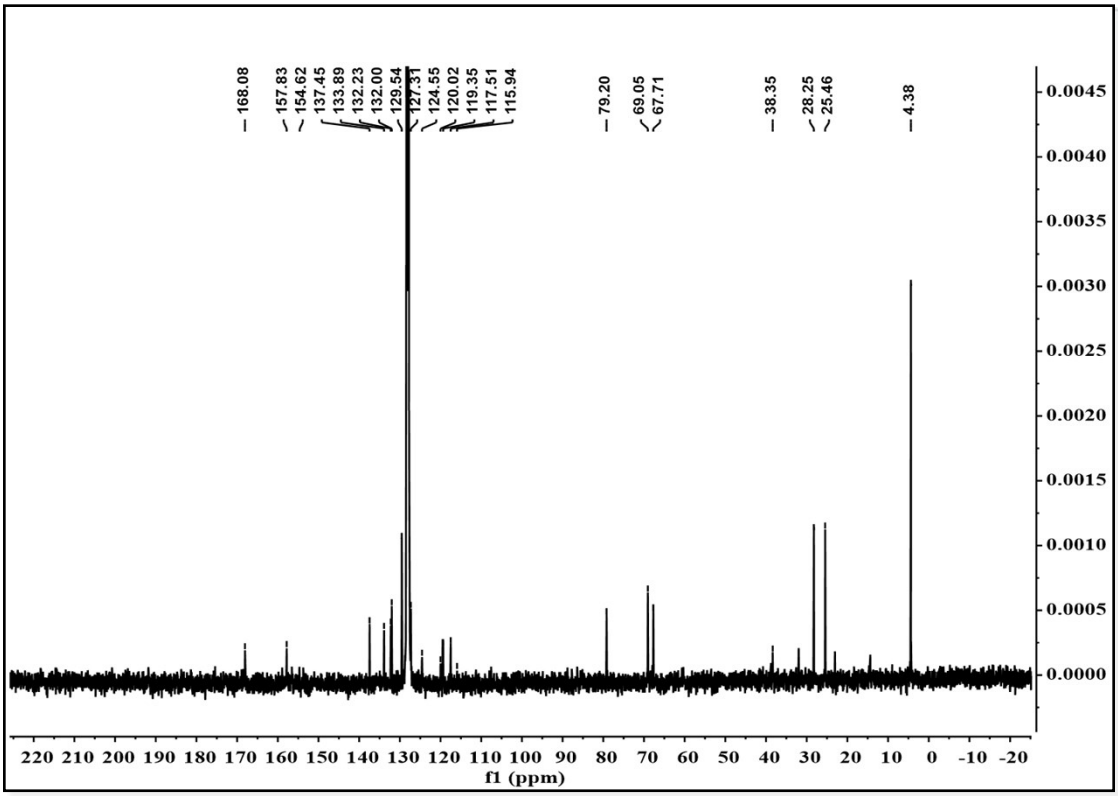

Figure S13 ^{13}C NMR spectrum of **S-Y** (101 MHz, C_6D_6, 25 °C)

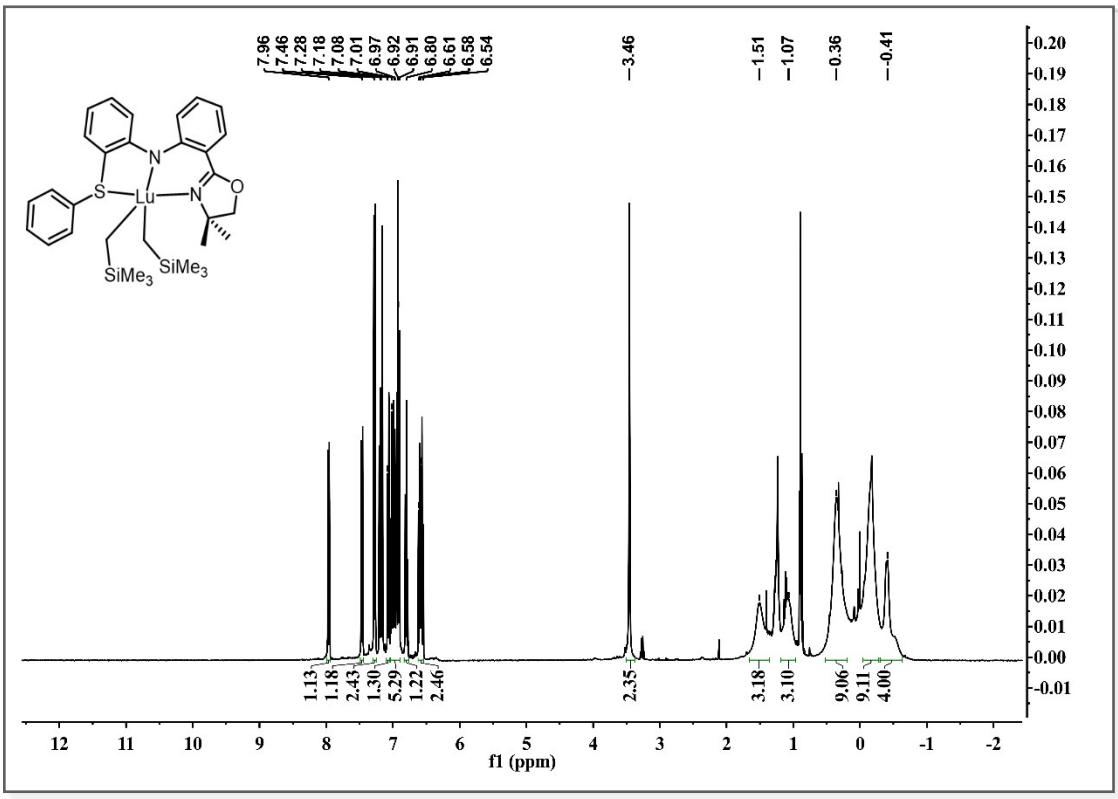

Figure S14 ^{1}H NMR spectrum of **S-Lu** (400 MHz, C_6D_6, 25 °C)

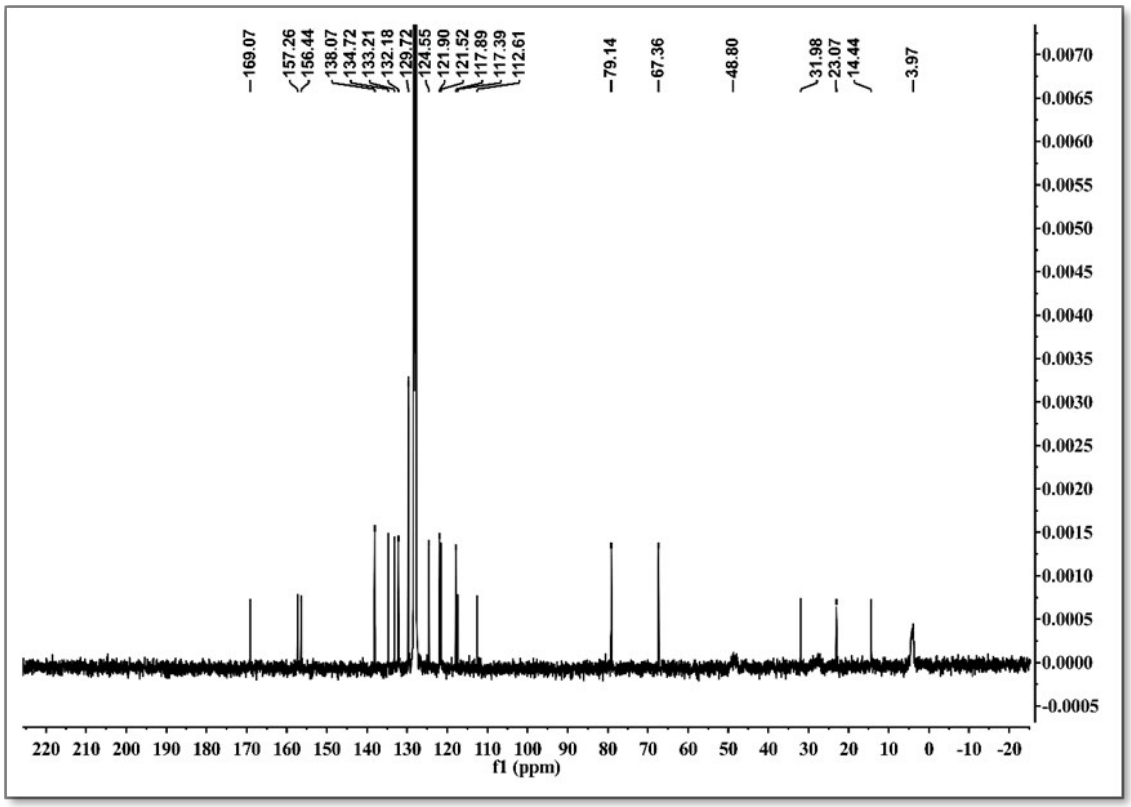

Figure S15 ^{13}C NMR spectrum of **S-Lu** (101 MHz, C_6D_6, 25 °C)

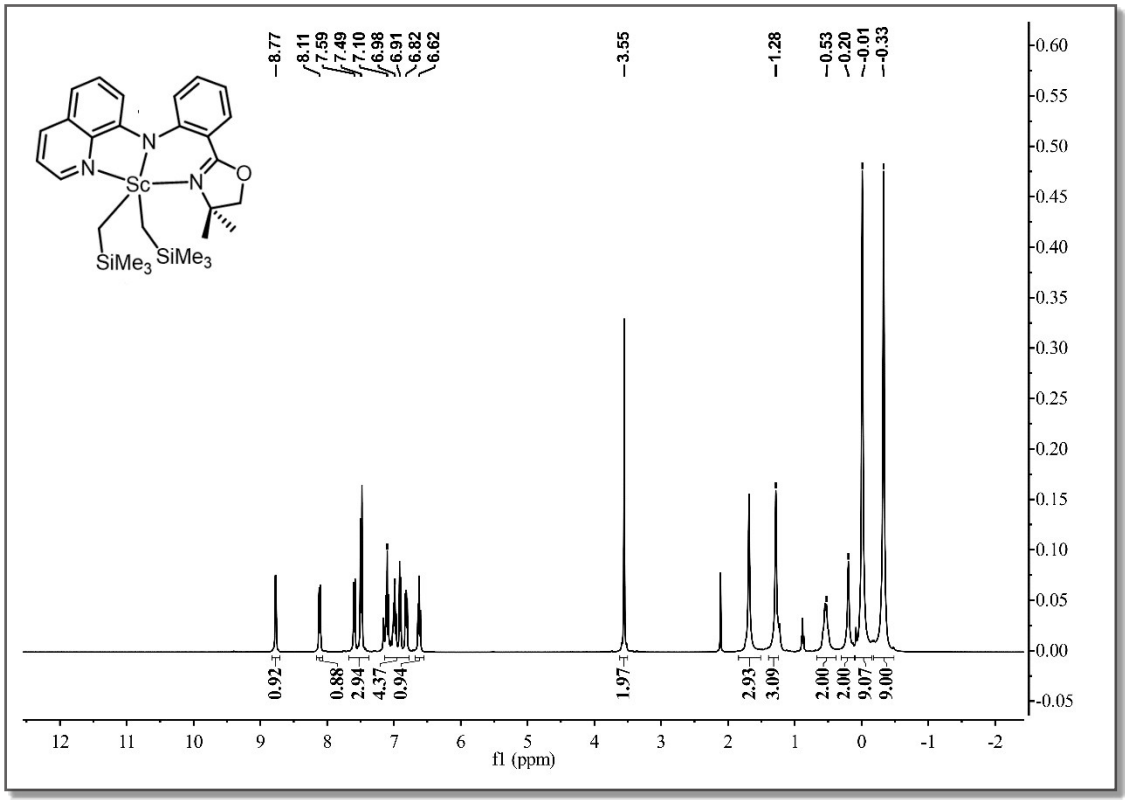

Figure S16 ^{1}H NMR spectrum of **N-Sc** (400 MHz, C_6D_6, 25 °C)

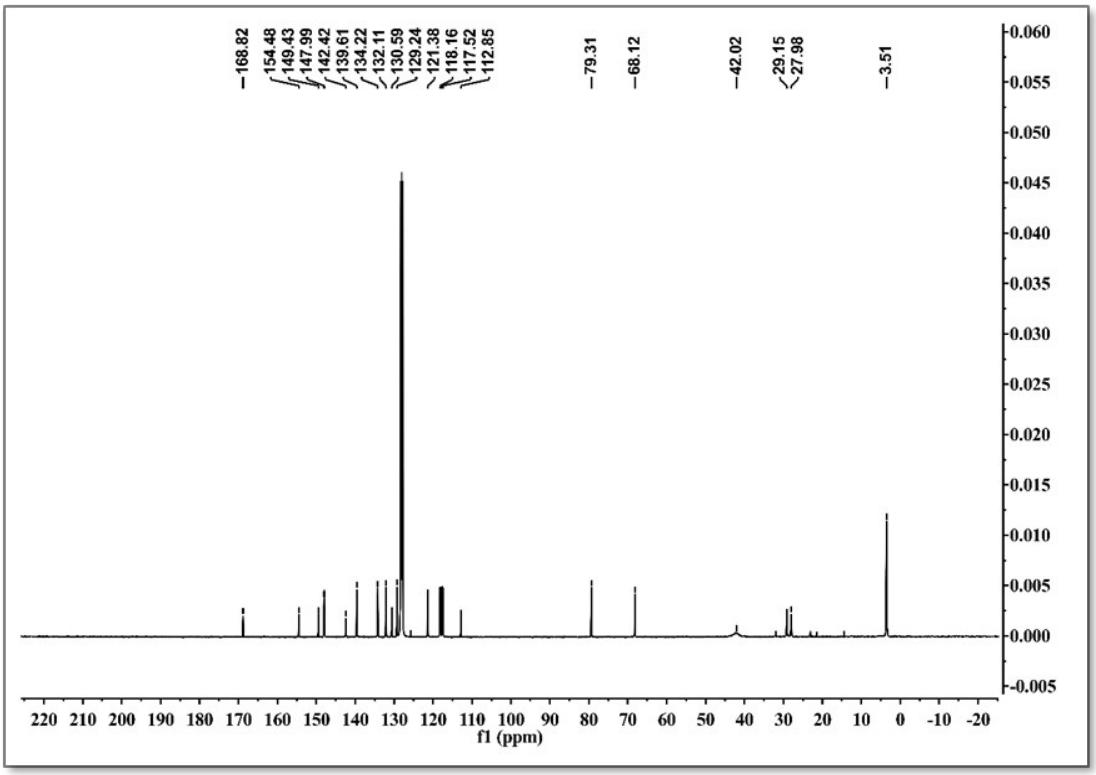

Figure S17 ^{13}C NMR spectrum of **N-Sc** (101 MHz, C_6D_6, 25 ℃)

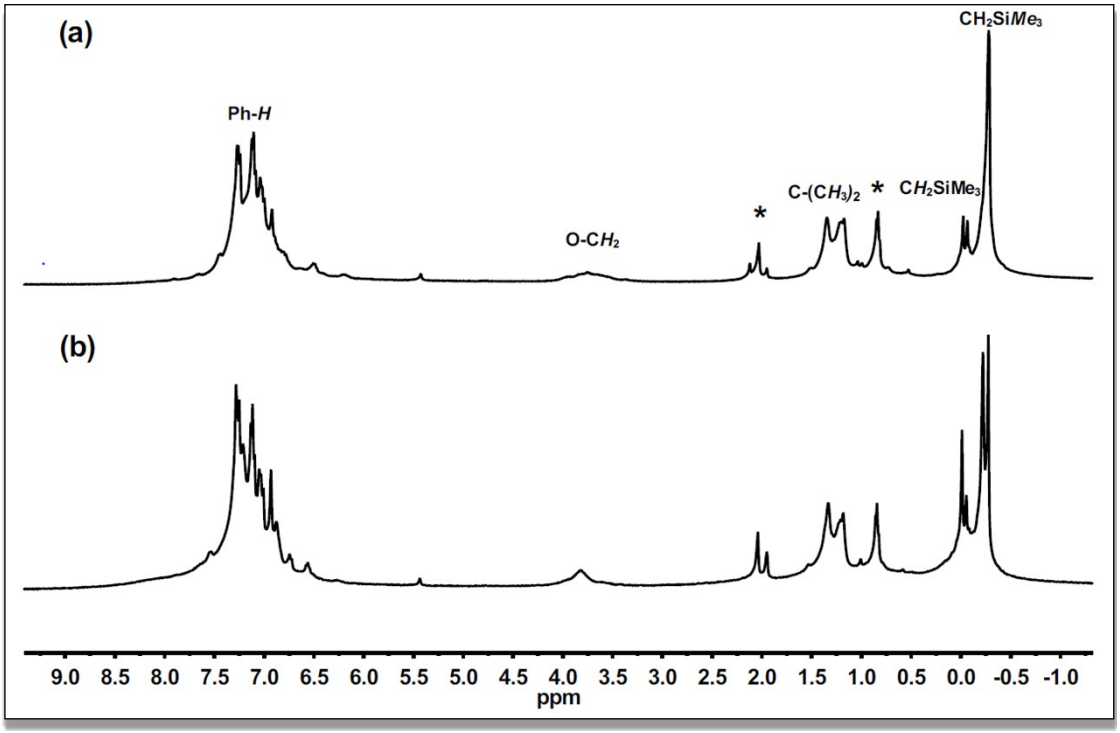

Figure S18 ^{1}H NMR spectra of rare-earth complexes with addition of borate $[Ph_3C][B(C_5F_5)_4]$.(**a**) **P-Lu** + $[Ph_3C][B(C_5F_5)_4]$; (**b**) **P-Y** + $[Ph_3C][B(C_5F_5)_4]$ (400 MHz, C_6D_5Br, 25 ^{o}C; * solvent)

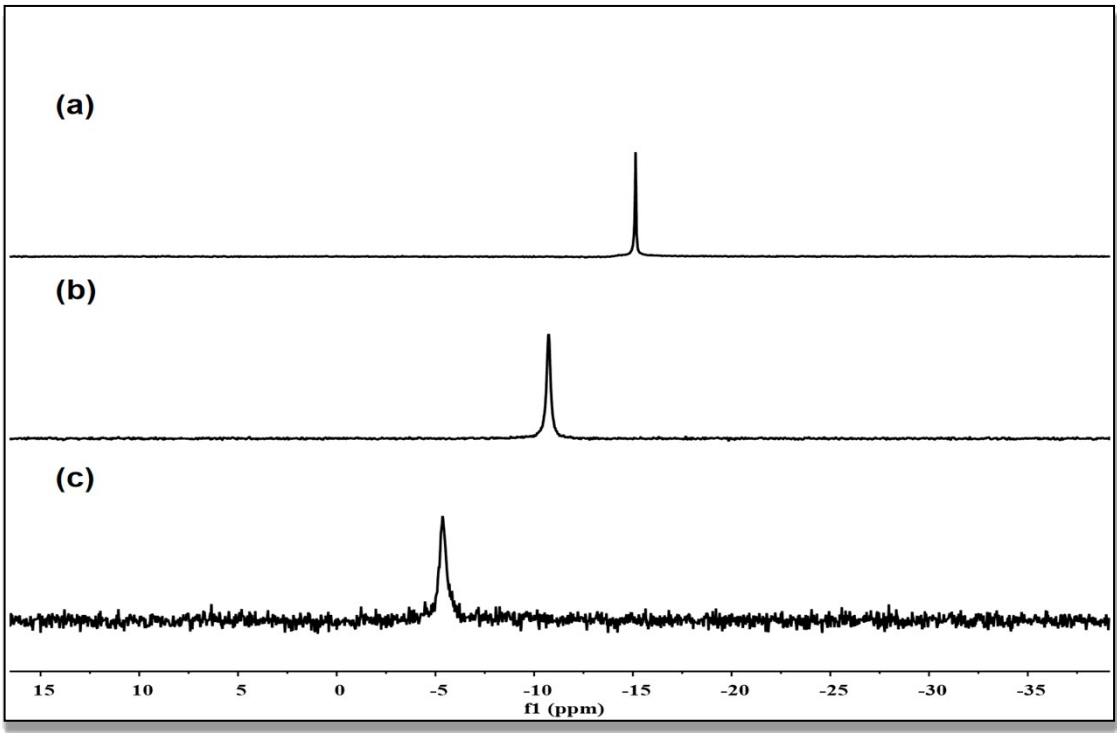

Figure S19 ^{31}P $\{^{1}H\}$ NMR spectrum of (a) **PNN** ligand (b) **P-Sc** (c) **P-Sc +** $[Ph_3C][B(C_5F_5)_4]$ (162 MHz, chlorobenzene, 25 ℃)

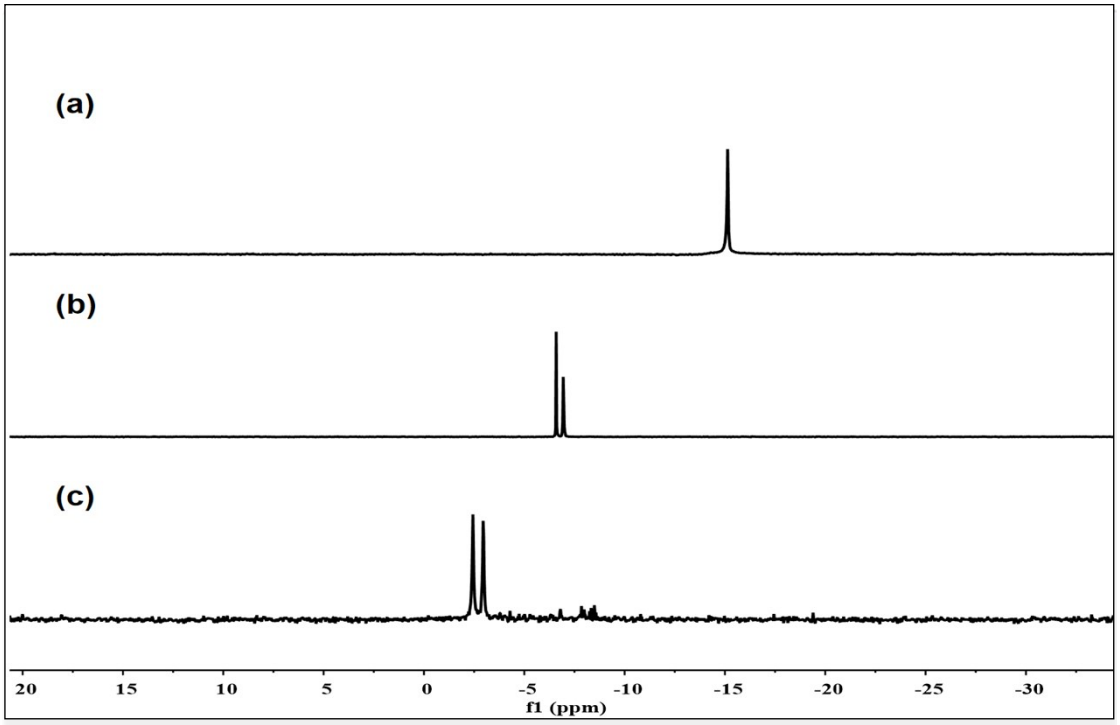

Figure S20 ^{31}P $\{^{1}H\}$ NMR spectrum of (a) **PNN** ligand (b) **P-Y** (c) **P-Y+** $[Ph_3C][B(C_5F_5)_4]$ (162 MHz, chlorobenzene, 25 ℃)

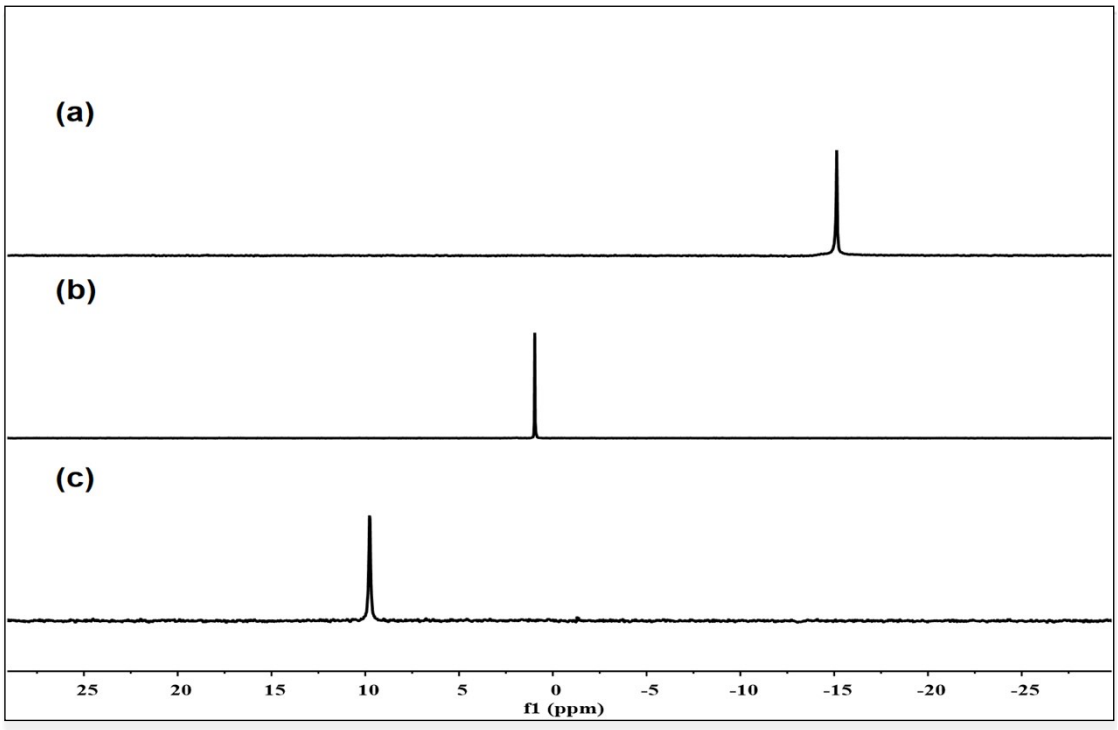

Figure S21 ^{31}P $\{^{1}H\}$ NMR spectrum of (a) **PNN** ligand (b) **P-Lu** (c) **P-Lu+** $[Ph_3C][B(C_5F_5)_4]$ (162 MHz, chlorobenzene, 25 ℃)

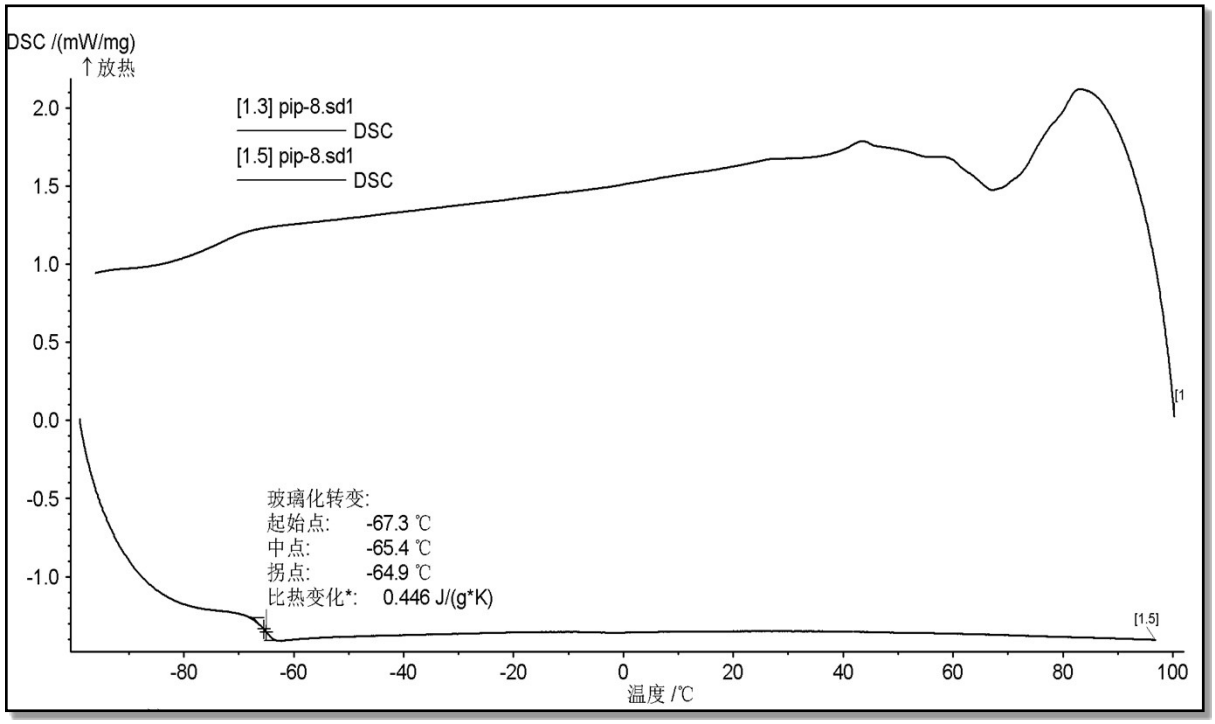

Figure S22 DSC thermograms of **PIP** polymer from entry 8 of **Table 1**.

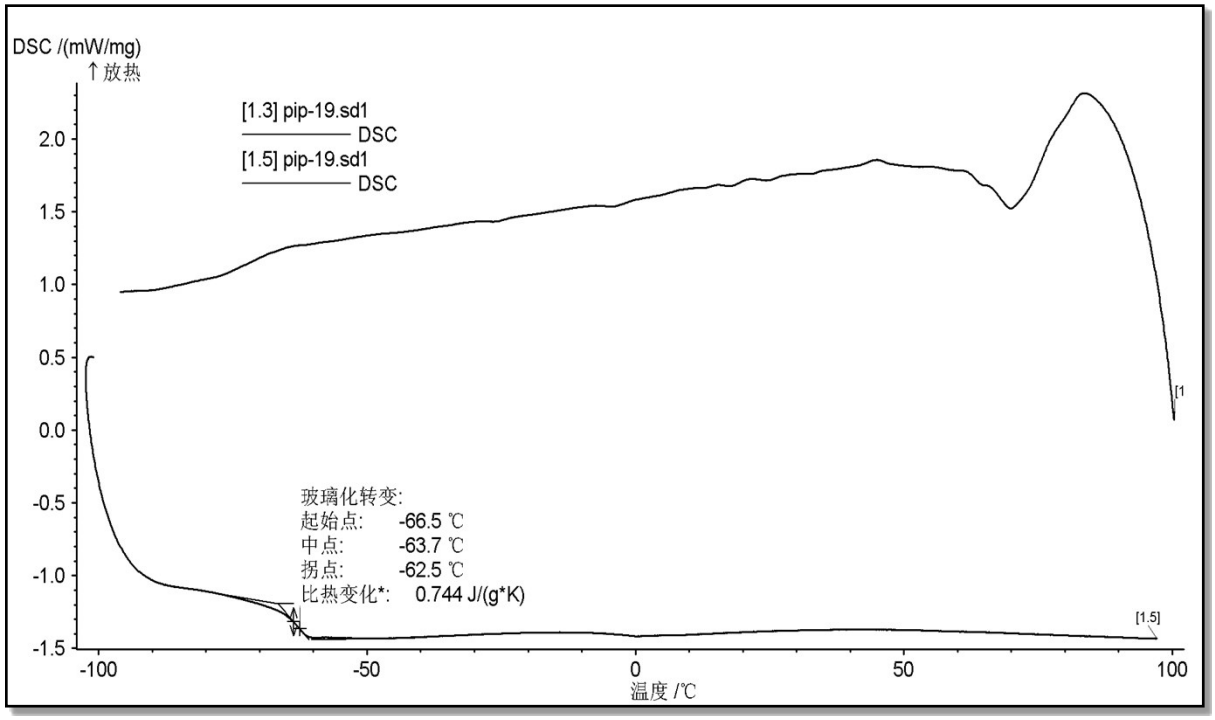

Figure S23 DSC thermograms of **PIP** polymer from entry 19 of **Table 1**.

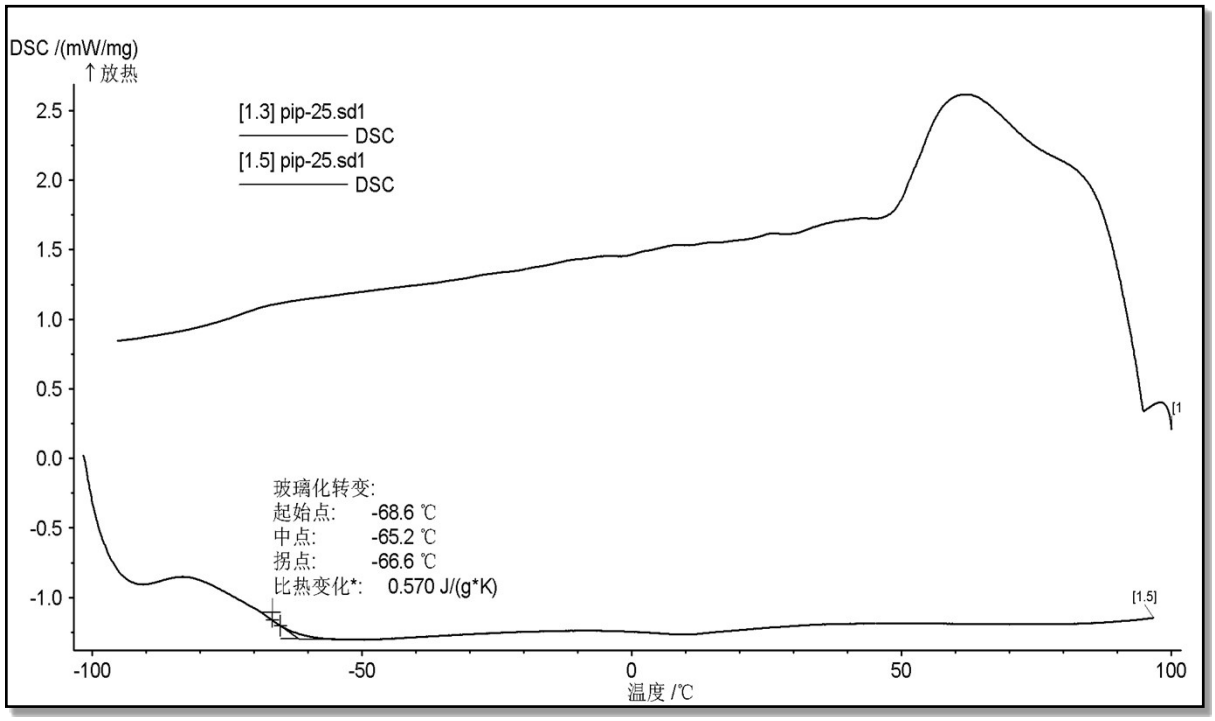

Figure S24 DSC thermograms of **PIP** polymer from entry 25 of **Table 1**.

Table S1. The data for P-Y, P-Lu, S-Y and S-Lu

Entry	cat.	co-cat.	t (min)	T (^{o}C)	[IP]/[Ln]	Conv. (%)	Microstructure (%)[b]			M_n[c]	M_w/M_n[c]	eff[d]
							cis-1,4	trans-1,4	3,4-			
1	P-Y	**A**	1	25	750:1	34	95.2	4.2	0.6	3.76	1.06	0.46
2	P-Y	**A**	1.5	25	750:1	48	88.7	9.7	1.6	4.65	1.05	0.53
3	P-Y	**A**	2.5	25	750:1	71	89.1	9.4	1.5	6.10	1.05	0.59
4	P-Y	**A**	3.5	25	750:1	85	87.3	11.4	1.3	6.88	1.06	0.63
5	P-Y	**A**	5	25	750:1	100	88.0	10.7	1.3	7.95	1.05	0.64
6	P-Y	**A**	4	25	300:1	100	87.4	11.5	1.1	3.79	1.06	0.54
7	P-Y	**A**	5	25	500:1	100	86.7	12.0	1.3	5.34	1.06	0.63
8	P-Y	**A**	10	25	1000:1	100	86.3	11.9	1.8	10.37	1.05	0.65
9	P-Y	**A**	15	25	1500:1	100	85.5	13.5	1.0	14.69	1.07	0.69
10	P-Y	**B**	5	25	750:1	77	85.8	13.1	1.1	nd	nd	nd
11	P-Lu	**A**	5	25	750:1	49	18.3	71.9	9.8	5.30	1.07	0.47
12	P-Lu	**A**	10	25	750:1	69	18.9	71.6	9.5	7.72	1.07	0.46
13	S-Y	**A**	90	25	750:1	68	86.8	13.7	0	6.22	1.02	0.56
14	S-Y	**A**	120	25	750:1	84	81.5	18.5	0	7.04	1.03	0.61
15	S-Lu	**A**	360	0	750:1	0	-	-	-	-	-	-

[a]activator: **A** = $[Ph_3C][B(C_5F_5)_4]$; [b]Determined by ^{13}C NMR and ^{1}H NMR. [c]Determined by GPC in THF at 40 ^{o}C against a polystyrene standard. [d] Initiation efficiency=M_n(calculated)/M_n(measured).

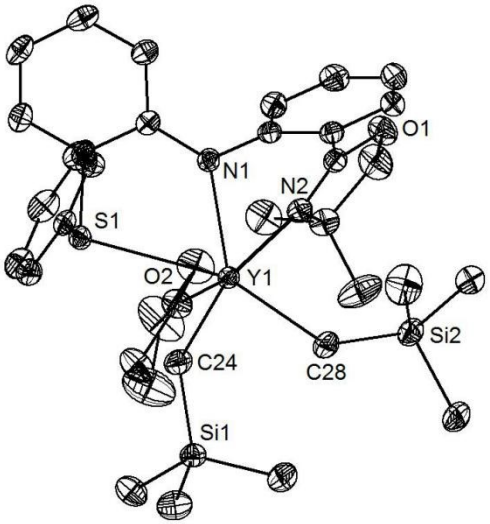

Figure S25 Molecular structure of **S-Y** (thermal ellipsoids at the 40 % probability level). Hydrogen atoms have been omitted for clarity. Selected bond distances (Å) and angles (deg): Y1-O2 2.3815(17), Y1-N1 2.3883(17), Y1-C28 2.396(2), Y1-C24 2.422(2), Y1-N2 2.4263(18), Y1-S1 2.9869(5), O2-Y1-N1 85.16(6), O2-Y1-C28 87.30(8), N1-Y1-C28 125.00(7), O2-Y1-C24 103.33(8), N1-Y1-C24 136.65(7), C28-Y1-C24 98.06(8), O2-Y1-N2 154.64(6), N1-Y1-N2 74.56(6), C28-Y1-N2 91.94(8), C24-Y1-N2 101.88(8), O2-Y1-S1 72.85(5), N1-Y1-S1 66.90(4), C28-Y1-S1 156.49(7)

Table S2. Summary of the crystallographic data for P-Sc, P-Y, P-Lu, S-Y and N-Sc

	P-Sc	**P-Y**	**P-Lu**	**S-Y**
Empirical formula	$C_{37}H_{48}ScN_2OPSi_2$	$C_{37}H_{48}YN_2OPSi_2$	$C_{37}H_{48}LuN_2OPSi_2$	$C_{35}H_{52.50}YN_2OSSi_2$
Formula weight	668.88	712.83	798.89	710.44
Temperature/K	173(2)	173(2)	173(2)	173(2)
Wavelength/ Å	1.34138	1.34138	0.71073	1.34138
Crystal system	Monoclinic	Monoclinic	Monoclinic	Triclinic
Space group	$P2_1/n$	P2(1)	$P2_1/n$	P-1
a/Å	10.8334(3)	10.9462(4)	10.8990(4)	10.9957(3)
b/Å	28.3891(8)	28.3973(10)	28.3514(11)	11.6568(3)
c/Å	13.0622(4)	13.2216(4)	13.1599(5)	14.7462(4)
α/°	90°	90	90	86.602(2)
β/°	109.6730(10)	109.9930(10)	109.8640(10)	83.774(2)
γ/°	90	90	90	85.085(2)
V/Å^3	3782.79(19)	3862.2(2)	3824.5(3)	1869.65(9)
Z	4	4	4	2
D_c/Mg m^{-3}	1.174	1.226	1.387	1.262
μ/mm^{-1}	1.924	2.212	2.715	2.372
F(000)	1424	1496	1624	751
Crystal size/mm^3	0.180 x 0.100 x 0.050	0.440 x 0.200 x 0.100	0.170 x 0.110 x 0.060	0.180 x 0.110 x 0.060
2θ range for data collection/°	3.407 to 57.022	3.378 to 56.998	1.795 to 27.156	4.125 to 57.998
Limiting indices(*hkl*)	-13, 13; -35, 31; -16, 16	-13, 13; -35, 35; -16, 16	-13, 13; -36, 36; -16, 16	-13, 13; -14, 14; -18, 18
Reflections collected	30846	120112	95764	22702
Independent reflections	7729	7915	8444	7884
R_{int}	0.0405	0.0734	0.0520	0.0385
Completeness to θ/°	53.594 (99.7 %)	53.594 (100 %)	25.242 (100 %)	53.594 (99.5 %)
Data/restraints/parameters	7729 / 0 / 405	7915 / 0 / 405	8444 / 0 / 405	7884 / 39 / 417
Goodness-of-fit on F^2	1.024	1.060	1.053	1.056
Final R indexes [I ≥ 2σ (I)]	R1 = 0.0323, wR2 = 0.0833	R1 = 0.0272, wR2 = 0.0684	R1 = 0.0190, wR2 = 0.0403	R1 = 0.0375, wR2 = 0.0944
Final R indexes [all data]	R1 = 0.0395, wR2 = 0.0882	R1 = 0.0304, wR2 = 0.0700	R1 = 0.0247, wR2 = 0.0425	R1 = 0.0403, wR2 = 0.0967
Largest diff. peak/hole / e Å^{-3}	0.293, -0.308	0.499, -0.630	0.482, -0.414	2.376, -0.631

$R_1 = \Sigma||Fo| - |Fc||/\Sigma|Fo|$; $wR_2 = [\Sigma w(F_o^2-F_c^2)^2/\Sigma w(F_o^2)^2]^{1/2}$

Computational details

All calculations were performed with the Gaussian 09 program.[1] The B3PW91 hybrid exchange-correlation functional was utilized for geometry optimization.[2-4] Each optimized structure was subsequently analyzed by harmonic vibration frequencies for characterization of a minimum (Nimag = 0) or a transition state (Nimag = 1) and providing thermodynamic data. The transition state structures are shown to connect the reactant and product on either side via intrinsic reaction coordinate (IRC) following. The 6-31G* basis set was considered for C, H, and N atoms, and the Si, P, Sc, Y, and Lu atoms were treated by the Stuttgart/Dresden effective core potential (ECP) and the associated basis sets.[5,6] The basis sets of Si and P were augmented with one *d*-polarization function (exponent of 0.284 and 0.387, respectively).[7] This basis set is denoted as "BSI". To obtain more reliable relative energies, the single-point calculations of optimized structures were carried out at the level of B3PW91-D3 (B3PW91 with Grimme's DFT-D3 correction)[8,9]/BSII, taking into account solvation effect of chlorobenzene with the SMD[10] solvation model. In the BSII, the 6-311+G(d,p) basis set was used for nonmetal atoms, while the basis sets together with associated pseudopotentials for Sc, Y, and Lu atoms are the same as that in geometry optimization. Therefore, unless otherwise mentioned, the free energy (ΔG, 298.15 K, 1 atm) in solution, which was used for description of energy profiles, was obtained from the solvation single-point calculation and the gas-phase Gibbs free energy correction. The 3D molecular structures displayed in this paper were drawn by using CYLview.[11]

(1) Frisch, M.; Trucks, G.; Schlegel, H.; Scuseria, G.; Robb, M.; heeseman, J.; Scalmani, G.; Barone, V.; Mennucci, B.; Petersson, G.; Nakatsuji, H.; Caricato, M.; Li, X.; Hratchian, H.; Izmaylov, A.; Bloino, J.; Zheng, G.; Sonnenberg, J.; Hada, M.; Ehara, M.; Toyota, K.; Fukuda, R.; Hasegawa, J.; Ishida, M.; Nakajima, T.; Honda, Y.; Kitao, O.; Nakai, H.; Vreven, T.; Montgomery, Jr.; Peralta, J.; Ogliaro, F.; Bearpark, M.; Heyd, J.; Brothers, E.; Kudin, K.; Staroverov, V.; Kobayashi, R.; Normand, J.; Raghavachari, K.; Rendell, A.; Burant, J.; Iyengar, S.; Tomasi, J.; Cossi, M.; Rega, N.; Milam, N.; Klene, M.; Knox, J.; Cross, J.; Bskken, V.; Adamo, C.; Jaramillo, J.; Gomperts, R.; Stratmann, R.; Yazyev, O.; Austin, A.; Cammi, R.; Pomelli, C.; Ochterski, J.; Marin, R.; Morokuma, K.; Zakrzewski, V.; Voth, G.; Salvador, P.; Dannenberg, J.; Dapprich, S.; Daniels, A.; Farkas, Ö.; Foresman, J.; Ortiz, J.; Cioslowski, J.; Fox, D. Gaussian 09, Revision A.02, Gaussian, Inc., Wallingford, CT. 2009.

(2) Becke, A. Density-functional thermochemistry. III. The role of exact exchange. *J. Chem. Phys.* **1993**, *98*, 5648–5653.

(3) Lee, C.; Yang, W.; Parr, R. Development of the Colic-Salvetti correlation-energy formula into a functional of the electron density. *Phys. Rev. B* **1988**, *37*, 785−789.

(4) Perdew, J.; Burke, K.; Wang, Y. Generalized gradient approximation for the exchange-correlation hole of a many-electron system. *Phys. Rev. B* **1996**, *54*, 16533−16539.

(5) Andrae, D.; H. U.; Dolg, M.; Stoll, H.; P, H. Energy-adjusted Ab initio pseudopotentials for the second and third row transition elements. *Theor. Chim. Acta* **1990**, *77*, 123−141.

(6) Martin, J.; Sundermann, A. Correlation consistent valence basis sets for use with the Stuttgart-Dresden-Bonn relativistic effective core potentials: The atoms Ga-Kr and In-Xe. *J. Chem.*

Phys. **2001**, *114*, 3408−3420.

(7) Höllwarth, A.; Böhme, M.; Dapprich, S.; Ehlers, A. W.; Gobbi, A.; Jonas, V.; Köhler, K. F.; Stegmann, R.; Veldkamp, A.; Frenking, G. A set of d-polarization functions for pseudo-potential basis sets of the main group elements Al-Bi and f-type polarization functions for Zn, Cd, Hg, *Chem. Phys. Lett.* **1993**, *208*, 237–240.

(8) Grimme, S.; Antony, J.; Ehrlich, S.; Krieg, H. A consistent and accurate ab initio parametrization of density functional dispersion correction (DFT-D) for the 94 elements H-Pu. *J. Chem. Phys.* **2010**, *132*, 154104–15424.

(9) Grimme, S. Accurate description of van der waals complexes by density functional theory including empirical corrections. *J. Comput. Chem.* **2004**, *25*, 1463–1473.

(10) Marenich, A.; Cramer, C.; Truhlar, D. Universal solvation model based on solute electron density and on a continuum model of the solvent defined by the bulk dielectric constant and atomic surface tensions. *J. Phys. Chem. B.* **2009**, *113*, 6378–6396.

(11) CYLview, 1.0b; Legault, C. Y., Université de Sherbrooke, 2009 (http://www.cylview.org)

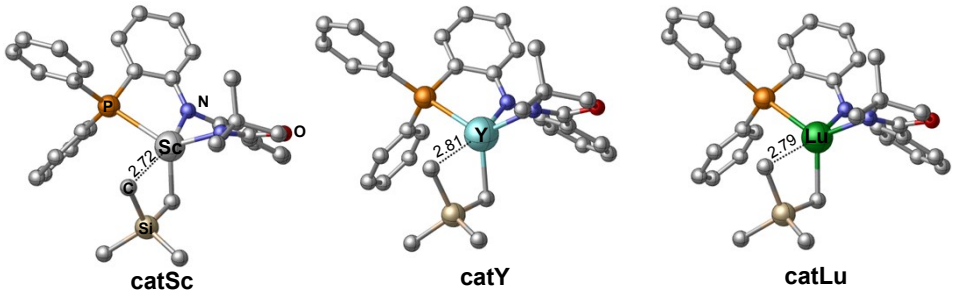

Figure S26 Optimized structures (distance in Å) of cationic species **catSc**, **catY**, and **catLu**, all hydrogen atoms are omitted for cl

Table S3 All related energy profiles for isoprene polymerization at chain initiation and propagation stages catalyzed by species **catSc**, **catY**, and **catLu**. Energies are relative to corresponding cationic species **catSc**, **catY**, and **catLu** and *trans*-monomer.

catY	Insertion fashions	**Y-C(1/2/3)**	**Y-TS(1/2/3)**	**Y-P(1/2/3)**	$\Delta G^{\ddagger}$/kcal mol^{-1}
The first monomer insertion	*trans-si*	–1.4	14.0	–17.4	15.4
	trans-re	–1.6	16.1	–18.2	17.7
	cis-re	0.9	15.3	–17.4	15.3
	cis-si	1.8	15.3	–14.5	15.3
The second monomer insertion	*trans-si-trans-si*	–14.1	–2.3	–34.8	15.1
	trans-si-trans-re	–14.6	–2.3	–35.4	15.1
	Y-TS2$_{anti-syn}$			–21.3	9.6
	trans-si-cis-re	–13.2	–5.2	–30.9	12.2
	cis-re-cis-re	–10.7	2.3	–23.7	19.7
	cis-re-cis-si	–9.2	–3.2	–28.4	14.2
The third monomer insertion	*trans-si-trans-si-trans-si*	–22.4	–8.2	–39.9	26.6
	trans-si-trans-re-trans-si	–23.1	–12.2	–42.0	23.2
	Y-TS3$_{anti-syn}$			–25.5	12.2
	trans-si-trans-re-cis-si	–20.5	–13.5	–37.7	21.9

	cis-re-cis-si-cis-re	–17.9	–10.9	–37.5	17.5
catLu	Insertion fashions	**Lu-C(1/2/3)**	**Lu-TS(1/2/3)**	**Lu-P(1/2/3)**	ΔG‡/kcal mol^{-1}
The first monomer insertion	*trans-si*	–2.6	14.2	–14.7	16.8
	trans-re	0.7	15.7	–14.4	15.7
	cis-re	2.3	14.3	–17.0	14.3
	cis-si	0.6	15.8	–12.0	15.8
The second monomer insertion	*trans-si-trans-re*	–14.1	–2.8	–32.7	11.9
	Lu-TS2$_{anti-syn}$			–20.7	7.9
	trans-si-cis-re	–11.1	–5.2	–28.6	9.5
	cis-re-cis-si	–6.8	–3.2	–27.1	13.8
The third monomer insertion	*trans-si-trans-re-trans-si*	–20.3	–11.6	–40.7	21.1
	Lu-TS3$_{anti-syn}$			–24.8	13.2
	trans-si-trans-re-cis-si	–19.8	–14.9	–38.0	17.8
	cis-re-cis-si-cis-re	–15.6	–9.4	–36.0	17.7
catSc	Insertion fashions	**Sc-C(1/2/3)**	**Sc-TS(1/2/3)**	**Sc-P(1/2/3)**	ΔG‡/kcal mol^{-1}
The first monomer insertion	*trans-si*	2.3	17.8	–16.4	17.8
	trans-re	2.5	18.3	–16.7	18.3
	cis-re	6.0	17.1	–18.4	17.1
	cis-si	3.6	18.5	–15.4	18.5
The second monomer insertion	*trans-si-trans-re*	–12.8	–1.3	–31.3	15.1
	cis-re-cis-si	–7.8	1.3	–23.9	19.7
The third monomer insertion	*trans-si-trans-re-trans-si*	–18.4	–9.8	–39.0	21.5
	trans-si-trans-re-cis-si	–17.3	–11.8	–36.5	19.5
	cis-re-cis-si-cis-re	–14.2	–8.3	–33.3	15.6

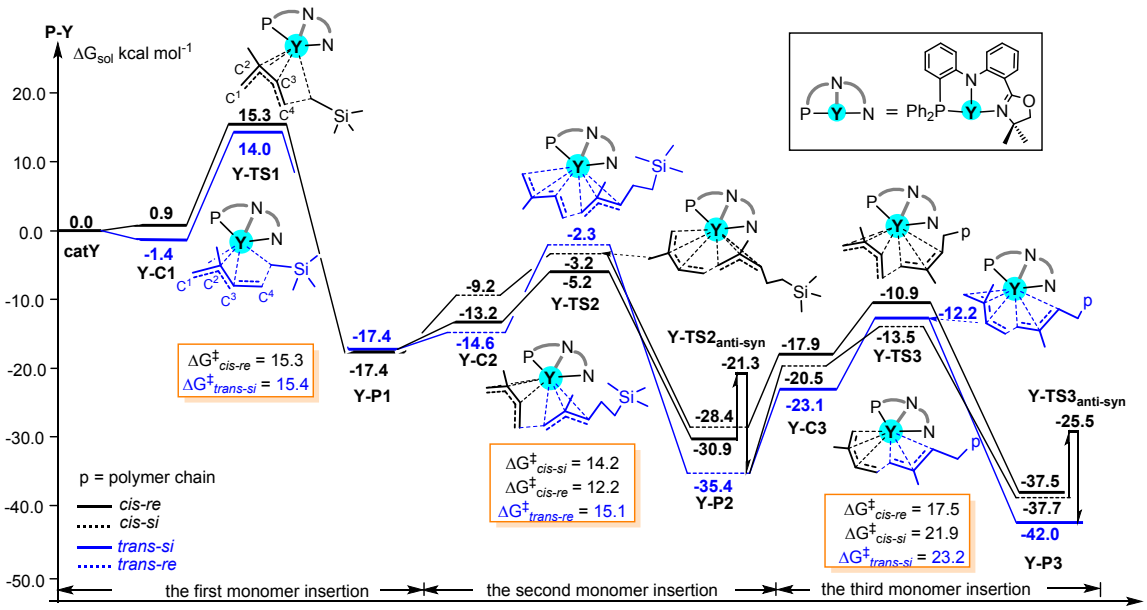

Figure S27 Energy profiles for the isoprene polymerization at chain initiation and propagation stages catalyzed by species **P-Y**. Energies are relative to corresponding cationic species **catY** and *trans-*

monomer.

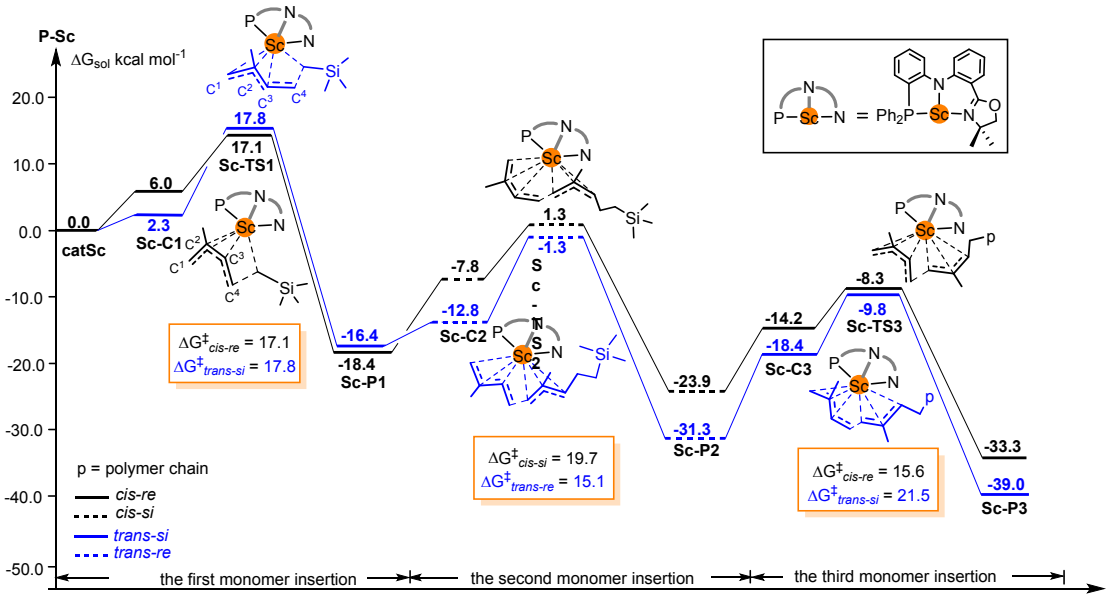

Figure S28 Energy profiles for the isoprene polymerization at chain initiation and propagation stages catalyzed by species **P-Sc**. Energies are relative to corresponding cationic species **catSc** and *trans*-monomer.

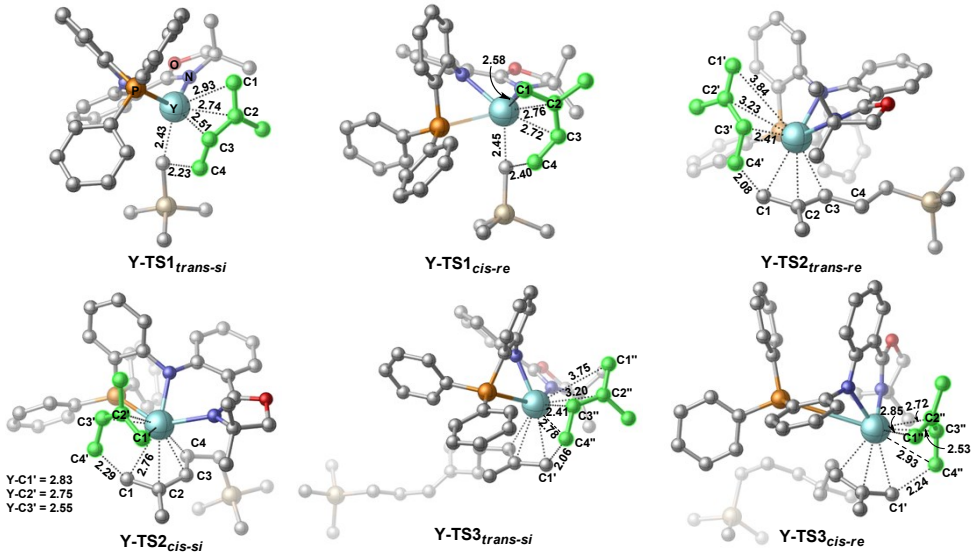

Figure S29 Optimized geometric structures (distance in Å) of key transition states involved in Fig. 6, all hydrogen atoms are omitted for clarity.

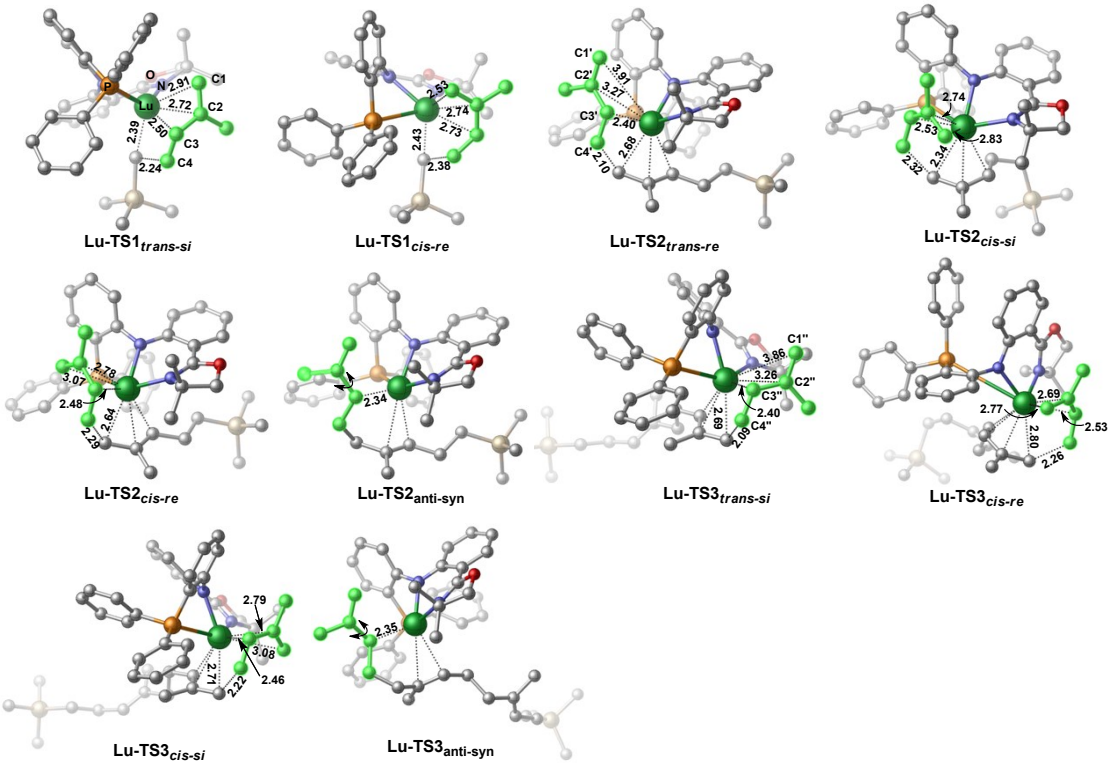

Figure S30 Optimized geometric structures (distance in Å) of key transition states involved in Fig. 7, all hydrogen atoms are omitted for clarity.